

Analytical solution for the surface states of antiferromagnetic topological insulator MnBi_2Te_4

Hai-Peng Sun,^{1, 2, 3} C. M. Wang,^{4, 2, 3} Song-Bo Zhang,⁵ Rui Chen,^{2, 3} Yue Zhao,² Chang Liu,² Qihang Liu,² Chaoyu Chen,² Hai-Zhou Lu,^{2, 3, *} and X. C. Xie^{6, 7, 8}

¹*Department of Physics, Harbin Institute of Technology, Harbin 150001, China*

²*Shenzhen Institute for Quantum Science and Engineering and Department of Physics, Southern University of Science and Technology (SUSTech), Shenzhen 518055, China*

³*Shenzhen Key Laboratory of Quantum Science and Engineering, Shenzhen 518055, China*

⁴*Department of Physics, Shanghai Normal University, Shanghai, 200234, China*

⁵*Institute for Theoretical Physics and Astrophysics, University of Wurzburg, D-97074 Wurzburg, Germany*

⁶*International Center for Quantum Materials, School of Physics, Peking University, Beijing 100871, China*

⁷*CAS Center for Excellence in Topological Quantum Computation, University of Chinese Academy of Sciences, Beijing 100190, China*

⁸*Beijing Academy of Quantum Information Sciences, West Building 3, No. 10, Xibeiwang East Road, Haidian District, Beijing 100193, China*

(Dated: March 8, 2022)

Recently, the intrinsic magnetic topological insulator MnBi_2Te_4 has attracted great attention. It has an out-of-plane antiferromagnetic order, which is believed to open a sizable energy gap in the surface states. This gap, however, was not always observable in the latest angle-resolved photoemission spectroscopy (ARPES) experiments. To address this issue, we analytically derive an effective model for the two-dimensional (2D) surface states by starting from a three-dimensional (3D) Hamiltonian for bulk MnBi_2Te_4 and taking into account the spatial profile of the bulk magnetization. Our calculations suggest that the diminished surface gap may be caused by a much smaller and more localized intralayer ferromagnetic order. In addition, we calculate the spatial distribution and penetration depth of the surface states, which indicates that the surface states are mainly embedded in the first two septuple layers from the terminating surface. From our analytical results, the influence of the bulk parameters on the surface states can be found explicitly. Furthermore, we derive a $\mathbf{k} \cdot \mathbf{p}$ model for MnBi_2Te_4 thin films and show the oscillation of the Chern number between odd and even septuple layers. Our results will be helpful for the ongoing explorations of the MnBi_xTe_y family.

Introduction.— A topological insulator has topologically protected conducting surface states and insulating interior [1–4]. When it is doped with magnetic impurities [5, 6], time reversal symmetry breaking can open a band gap in its surface states. The band gap is essential for the realization of the quantized anomalous Hall effect [6, 7], which hosts dissipationless chiral edge states with potential applications in future devices. However, as magnetic impurities inevitably introduce inhomogeneity and disorder, the temperature at which the quantized anomalous Hall effect can be observed is typically low (< 2 K) [8, 9]. The working temperature may be increased by using the magnetic extension method [10, 11] or intrinsic magnetic topological insulators [12–15], where magnetism is part of the crystal. Recently, an intrinsic antiferromagnetic (AFM) topological insulator MnBi_2Te_4 was predicted [16–18] and has been verified by experiments [16, 19–25]. Quantum anomalous Hall effect [26], axion insulator to Chern insulator transition [27], and high Chern number quantum Hall effect without Landau levels [28] have been reported in the MnBi_2Te_4 thin films. Nevertheless, the latest experiments imply that the topological surface states in a bulk crystal of MnBi_2Te_4 may be gapless [23–25], in contrast to the earlier calculations

and observations [16–22, 29–33] (see Table I).

To understand why there is a wide range of the surface gap in the measurements, we derive analytically the effective model for the surface states as the analytical model can address the surface of a bulk crystal in terms of explicit expressions. Particularly, in the derivation we take into account the spatial profile of the bulk magnetization (Fig. 1). We show how the surface gap depends on the amplitude and acting range of the intralayer ferromagnetic order. We also summarize the estimated amplitude of the intralayer ferromagnetic order m_0 from the surface gap observed in the experiments (see Table I). In addition, we calculate the spatial distribution and penetration depth of the surface states, which indicates that the surface states are mainly embedded in the first two septuple layers from the terminating surface. Although we use the envelope function within the $\mathbf{k} \cdot \mathbf{p}$ approach, the order of magnitude of the penetration depth is consistent with the results obtained by the *ab initio* calculations [34]. We also derive a $\mathbf{k} \cdot \mathbf{p}$ model for MnBi_2Te_4 thin films. Our results will be helpful for the ongoing explorations of the MnBi_xTe_y family.

Effective model for surface states.— The electronic structure of semi-infinite crystals can be calculated ex-

TABLE I. The gaps of the surface states of the AFM MnBi₂Te₄ based on density functional theory (DFT) and angle-resolved photoemission spectroscopy (ARPES) and the estimated amplitude of the intralayer ferromagnetic order m_0 from the experiments, where Eq. (5) has been used and $n = 1$ has been taken as an example.

Reference	Method	Surface gap (meV)	m_0 (meV)
Otrokov <i>et al.</i> [16]	DFT	88	
Otrokov <i>et al.</i> [16]	ARPES	70	218
Lee <i>et al.</i> [33]	ARPES	85	265
Zeugner <i>et al.</i> [32]	ARPES	100	311
Chen <i>et al.</i> [20]	ARPES	< 25	< 78
Hao <i>et al.</i> [23]	ARPES	< 3	< 9
Li <i>et al.</i> [22]	ARPES	< 13.5	< 42
Chen <i>et al.</i> [24]	ARPES	< 2.5	< 8
Swatek <i>et al.</i> [25]	ARPES	< 2	< 6
Shikin <i>et al.</i> [34]	ARPES	15 – 67	47 – 209

plicitly by the *ab initio* calculations that include Green's functions. As an alternative way to calculate the surface states, the $\mathbf{k} \cdot \mathbf{p}$ approach can give qualitatively (even quantitatively) consistent results with the *ab initio* calculations [34]. A general approach for heterostructures containing the magnetically modulated doped topological insulator films can be found in Ref. [35], which provides a consistent interpretation of the well-known experimental findings [8]. Starting from the three-dimensional (3D) Hamiltonian for the AFM1 (polarized along the z direction) state of MnBi₂Te₄ [17], we derive the effective model for surface states in a semi-infinite geometry. The technique [4] that we are using has been shown effective in the predictions of the quantum spin Hall effect in topological insulator thin films [36–38] and 3D quantum Hall effect in topological semimetals [39, 40]. The 3D Hamiltonian of AFM MnBi₂Te₄ reads

$$\mathcal{H}(\mathbf{k}) = \epsilon_0(\mathbf{k}) + \begin{bmatrix} M(\mathbf{k}) & A_1 k_z & 0 & A_2 k_- \\ A_1 k_z & -M(\mathbf{k}) & A_2 k_- & 0 \\ 0 & A_2 k_+ & M(\mathbf{k}) & -A_1 k_z \\ A_2 k_+ & 0 & -A_1 k_z & -M(\mathbf{k}) \end{bmatrix} + H_X, \quad (1)$$

where $k_{\pm} = k_x \pm i k_y$, $\epsilon_0(\mathbf{k}) = C_0 + D_1 k_z^2 + D_2 (k_x^2 + k_y^2)$ and $M(\mathbf{k}) = M_0 - B_1 k_z^2 - B_2 (k_x^2 + k_y^2)$. C_0 , D_i , M_0 , B_i and A_i are model parameters, where $i = 1, 2$. The basis of the Hamiltonian is $\{|P1_z^+, \uparrow\rangle, |P2_z^-, \uparrow\rangle, |P1_z^+, \downarrow\rangle, |P2_z^-, \downarrow\rangle\}$. Conventionally, the exchange field is treated as a constant m_0 in H_X . Unlike the previous works [36, 37], we take into account the spatial profile of the exchange field in the AFM MnBi₂Te₄ for a realistic study. For simplicity, we consider the profile of the exchange field in terms of the sinusoidal function, and the exchange field

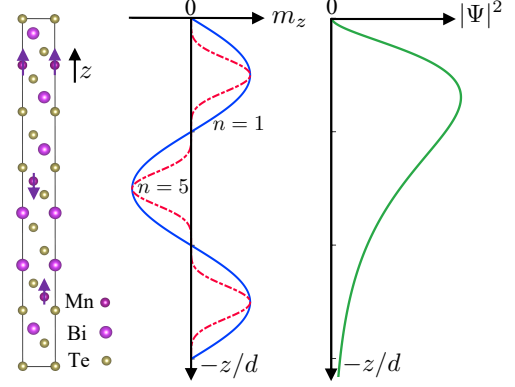


FIG. 1. (Left) Septuple layers of MnBi₂Te₄ [41]. The purple arrows denote the direction of the ferromagnetic order in the Mn atomic layer. (Middle) The assumed profile of the bulk magnetization $m_z \sim \sin^n(\pi z/d)$. n is an odd integer that controls the acting range of the intralayer ferromagnetic order and is the only tuning parameter in the calculation. d is the thickness of a septuple layer. (Right) The distribution of the envelope function Ψ of the surface states.

H_X reads

$$H_X = -m_0 \sin^n\left(\frac{\pi}{d}z\right) \sigma_z \otimes \tau_0, \quad (2)$$

where m_0 is the amplitude of the intralayer ferromagnetic order, d is the thickness of a septuple layer, σ_z is the z Pauli matrix for the spin degrees of freedom, τ_0 is a 2×2 unit matrix for the orbital degrees of freedom, and the magnetization energy along the z direction $m_z = -m_0 \sin^n(\pi z/d)$ is illustrated in Fig. 1 for different n . The odd integer n is used to model the localization of the intralayer ferromagnetic order. A larger n indicates that the intralayer ferromagnetic order is more localized. Here, we focus on the out-of-plane magnetic moments according to the neutron diffraction results [42].

We now consider a surface located at $z = 0$ and derive the effective model for the surface states, as shown in Fig. 1. First, we find the solutions to the surface states at $k_x = k_y = 0$ (the Γ point), where the Hamiltonian becomes two 2×2 blocks, denoted as $h(A_1)$ and $h(-A_1)$, respectively. The trial solution to the eigen equation $h(A_1)\Psi = E\Psi$ can be written as $\Psi = (a, b)^T e^{\lambda z}$, where a , b , and λ are the coefficients and E is the eigenenergy. There are two solutions to λ , denoted as λ_1 and λ_2 , and the general solution is a linear combination of them, $\Psi(z) = \sum_{i=1}^2 (a_i, b_i)^T e^{\lambda_i z}$. For simplicity, we assume open boundary conditions on the surfaces. We note, however, the main features of surface states, such as their attenuation in the bulk, are generic and remain the same if we impose different boundary conditions. Thus, the envelope function Ψ vanishes at $z = 0$ and $z = -\infty$, which are applied to the general solution to obtain the eigenenergy at the Γ point $E_0 = C_0 + M_0 D_1 / B_1$ and the

envelope function

$$\Psi^\uparrow(z) \sim \begin{bmatrix} iA_1 \\ -D_- \lambda_+ \end{bmatrix} (e^{\lambda_1 z} - e^{\lambda_2 z}) \quad (3)$$

up to a normalization factor with $D_- = D_1 - B_1$, and $\lambda_+ = \lambda_1 + \lambda_2$. Replacing A_1 with $-A_1$ can give the eigenenergy and the envelope function $\Psi^\downarrow(z)$ of the other block $h(-A_1)$, which is degenerate with $h(A_1)$ when there is no magnetization.

Next, we project the Hamiltonian at $\{k_x, k_y\} \neq 0$ into the basis expanded by $\Phi_1 = [\Psi^\uparrow(z), 0]^T$ and $\Phi_2 = [0, \Psi^\downarrow(z)]^T$, and obtain the 2D effective Hamiltonian for surface states localized at the surface,

$$H_{\text{surface}} = E_0 - Dk^2 + \begin{bmatrix} m & i\gamma k_- \\ -i\gamma k_+ & -m \end{bmatrix}, \quad (4)$$

where $D = \tilde{B}_2 - D_2$, $\tilde{B}_2 = B_2 \langle \Psi^\uparrow(z) | \sigma_z | \Psi^\uparrow(z) \rangle$, and $\gamma = -iA_2 \langle \Psi^\uparrow(z) | \sigma_x | \Psi^\downarrow(z) \rangle$. Note that this effective model is valid only in the vicinity of the Γ point. m is the effective magnetic moment. It can be found explicitly as [43]

$$m = m'_0 n! \pi^n d \left\{ \frac{2}{\prod_{j=1}^{\frac{n+1}{2}} \{d^2 \lambda_+^2 + [(2j-1)\pi]^2\}} \right. \\ \left. - \sum_{i=1}^2 \frac{1}{\prod_{j=1}^{\frac{n+1}{2}} \{4d^2 \lambda_i^2 + [(2j-1)\pi]^2\}} \right\} \quad (5)$$

for an arbitrary odd integer n , where the parameter $m'_0 = -m_0 (A_1^2 + D_-^2 |\lambda_+|^2) |C|^2$ and C is the normalization factor.

Gap and penetration depth of surface states.—The two energy bands of the effective model, Eq. (4), are given by $E_{\text{surface}}^\pm = E_0 - Dk^2 \pm \sqrt{m^2 + \gamma^2 k^2}$, which shows that the surface states open a gap of magnitude $2|m|$ at the Γ point. Using Eq. (5), we calculate the effective magnetic moment m for increasing odd integers $n \in \{1, 3, 5, \dots\}$ and display m as functions of different model parameters in Figs. 2(a)–2(d). Figure 2(a) shows that the effective magnetic moment m is reduced when the intralayer ferromagnetic order m_0 becomes smaller or more localized (for larger n). In this sense, our calculations suggest that the diminished surface gap may be caused by a much smaller and more localized intralayer ferromagnetic order. It is worth mentioning that Shikin and collaborators proposed that the structural changes of the surface may cause the surface states moving inward, which will also result in a reduced effective magnetic moment [34, 44].

Besides, we calculate the spatial distribution $|\Psi(z)|^2$ and hence the penetration depth of surface states $\xi = |\langle \Psi | z | \Psi \rangle|$, using the parameters obtained by *ab initio* calculations [17]. As illustrated in Fig. 2(e)–2(h), the surface states are well localized at the surface, which have already been probed by the experiments [45, 46]. Importantly, we find that the penetration depth ξ is about 16.2

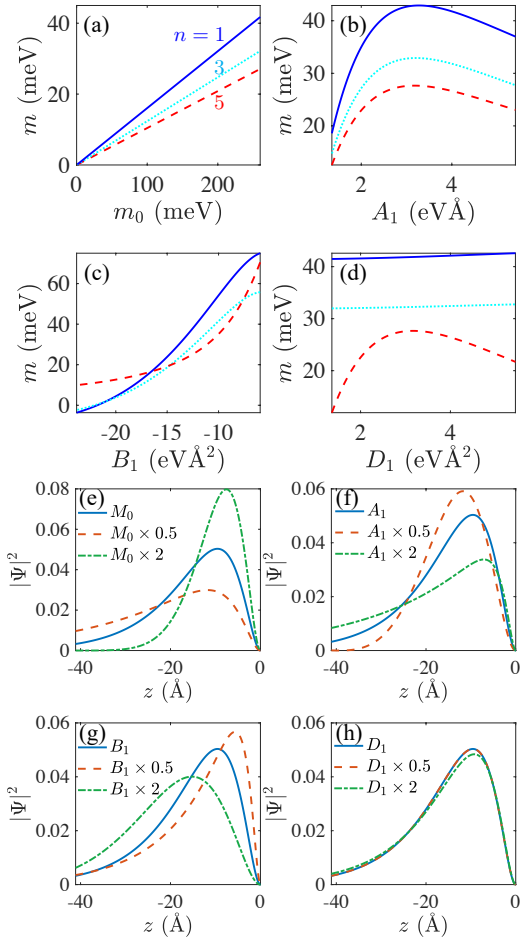


FIG. 2. (a) The relation between the effective magnetic moment m and the amplitude of the intralayer ferromagnetic order m_0 for different m_z profiles in Fig. 1. [(b)–(d)] The influence of the variation of the parameters A_1 , B_1 , and D_1 on the effective magnetic moment m , respectively. The blue solid, cyan dotted, and red dashed lines represent $n = 1, 3$, and 5, respectively. [(e)–(h)] The influence of the variation of the parameters M_0 , A_1 , B_1 , and D_1 on the distribution of the surface states, respectively. The parameters are adopted from *ab initio* calculations [17], $C_0 = -0.0048$ eV, $D_1 = 2.7232$ eV Å 2 , $D_2 = 17.0000$ eV Å 2 , $A_1 = 2.7023$ eV Å, $A_2 = 3.1964$ eV Å, $M_0 = -0.1165$ eV, $B_1 = -11.9048$ eV Å 2 , $B_2 = -9.4048$ eV Å 2 , and $m_0 = 0.26$ eV.

Å, which is larger than the thickness of a septuple layer (about 13.7 Å). This indicates that the surface states have already extended to the second septuple layer. Note that the penetration depth we estimated by using the envelope function is consistent with the results obtained by *ab initio* calculations [34, 47].

Influences of the bulk on the surface gap.—The parameters of the bulk Hamiltonian in Eq. (1), which are extracted from the *ab initio* calculations [17], can change with external conditions, such as mechanical exfoliation, defects, or doping. Therefore, we study the influence of the variation of the bulk parameters on the effective mag-

netic moment m and surface gap $2|m|$. As A_1 increases, m first increases and then decreases for different n , as shown in Fig. 2(b). The decrease of m is due to the cancellation of the opposite magnetization between odd and even septuple layers, as the surface envelope function becomes more extended with increasing A_1 , as shown in Fig. 2(f). By contrast, with increasing B_1 , m increases first slowly and then abruptly for $n = 5$ and there are transitions from negative to positive m for $n = 1$ and 3, as illustrated in Fig. 2(c). With increasing D_1 , m increases slowly for $n = 1$ and 3. Nevertheless, for $n = 5$, m first increases and then decreases, as illustrated in Fig. 2(d). The change of m can also be understood from the distribution of the envelope function. As B_1 increases, the surface states move towards the surface plane, as depicted in Fig. 2(g). By contrast, as M_0 or A_1 increases, the surface states move away from the surface plane, as depicted in Figs. 2(e) and 2(f). In addition, as D_1 increases, the distribution of the surface states only changes slightly, as shown in Fig. 2(h).

Effective model for MnBi₂Te₄ thin films.— Above, we have discussed the gap at a single open surface in a semi-infinite geometry. Now, we turn to discuss the surface gap in a thin film with both top and bottom open surfaces. First, we derive the $\mathbf{k} \cdot \mathbf{p}$ model for MnBi₂Te₄ thin films. Following the same procedure as described above, we obtain the effective Hamiltonian for MnBi₂Te₄ thin films, which reads [43]

$$H_{\text{film}} = E_0 - Dk^2 + \begin{bmatrix} h(k) + m_1 & i\gamma k_- & m_2 & 0 \\ -i\gamma k_+ & -h(k) - m_3 & 0 & -m_2 \\ m_2 & 0 & -h(k) + m_3 & i\gamma k_- \\ 0 & -m_2 & -i\gamma k_+ & h(k) - m_1 \end{bmatrix} \quad (6)$$

where $E_0 = (E_+ + E_-)/2$, E_+ , and E_- are the eigenenergies at the Γ point, $h(k) = \Delta/2 - bk^2$ with $k^2 = k_x^2 + k_y^2$, $\Delta = E_+ - E_-$ is the finite-size gap, and m_i is the effective magnetic moment with $i = 1, 2, 3$. The eigenenergies of the surface states for even septuple layers are found as $E_{\text{even}} = E_0 - Dk^2 \pm \sqrt{(\Delta/2 - bk^2)^2 + \gamma^2 k^2 + m_2^2}$, which is two-fold degenerate due to $P_2\Theta$ symmetry [18], as shown in Fig. 3(a). At the Γ point, the surface gap for even septuple layers is $2\sqrt{(\Delta/2)^2 + m_2^2}$. It decreases as the thickness grows because both the finite-size gap Δ [Fig. 3(e)] and the effective magnetic moment m_2 [Fig. 3(d)] decrease with growing thickness. The surface gap and the effective magnetic moment m_2 finally saturate for larger N_L , as shown in Figs. 3(c) and 3(d). The eigenenergies of the surface states for odd septuple layers are found as $E_{\text{odd}} = E_0 - Dk^2 + s(m_1 - m_3)/2 \pm \sqrt{[\Delta/2 - bk^2 + s(m_1 + m_3)/2]^2 + \gamma^2 k^2}$ with $s = \pm 1$, which has no degeneracy due to the breaking of Θ and $P_2\Theta$ symmetry [18], as shown in Fig. 3(b). At the Γ point, the surface gap for odd septuple layers is $2\sqrt{[\Delta/2 + (m_1 + m_3)/2]^2}$. For $n = 1$ and $n = 5$, the

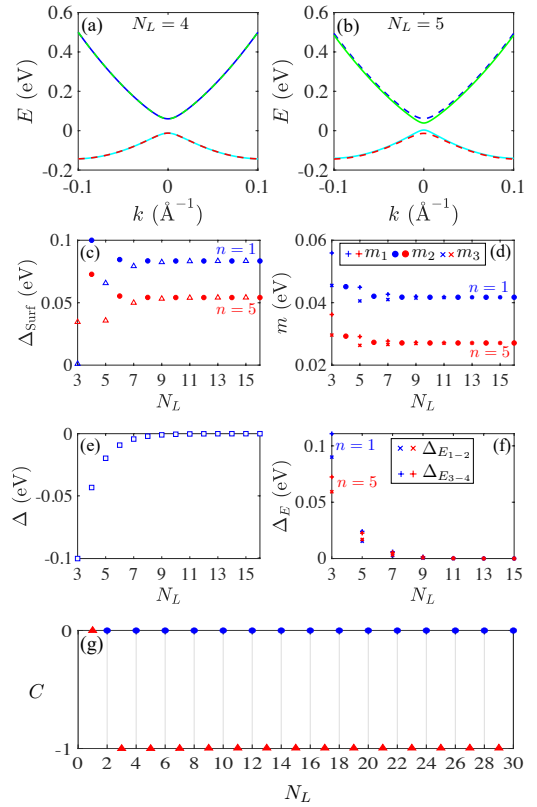


FIG. 3. The energy dispersion of even and odd septuple layers for (a) $N_L = 4$ and (b) $N_L = 5$. (c) The relation between the surface gap Δ_{Surf} and the number of septuple layers N_L for different m_z profiles in Fig. 1. The blue solid circles and empty triangles represent $n = 1$ and red solid circles and empty triangles represent $n = 5$, respectively. (d) The effective magnetic moments $m_{1,2,3}$ as functions of N_L for different m_z profiles in Fig. 1. The blue plus signs, crosses, and solid circles represent $n = 1$ and red plus signs, crosses, and solid circles represent $n = 5$, respectively. (e) The finite-size gap Δ versus N_L . (f) The energy difference of the upper two bands $\Delta_{E_{1-2}}$ and the energy difference of the lower two bands $\Delta_{E_{3-4}}$ versus N_L . (g) The Chern number C versus N_L . For even N_L , the Chern number is zero. For odd $N_L \geq 3$, the Chern number is -1 . The parameters are the same as in Fig. 2.

surface gap increases with growing N_L , and finally saturates for larger N_L . For the effective magnetic moment m_3 , it first decreases, then increases, and finally saturates for larger N_L , as shown in Figs. 3(c)–(d). Besides, the energy difference at the Γ point between the upper two bands $\Delta_{E_{1-2}}$ is different from that of the lower two bands $\Delta_{E_{3-4}}$ for odd septuple layers when $N_L < 11$, due to the difference between m_1 and m_3 , as shown in Figs. 3(d) and 3(f). The Chern number is zero for all the even septuple layers and $N_L = 1$ odd septuple layer, and is -1 for odd septuple layers with $N_L \geq 3$, as shown in Fig. 3(g). The oscillation of the Chern number in Fig. 3(g) is consistent with the nature of intrinsic antiferromagnetic topological insulators [17, 18, 29]. Note that $m_0 = 0.26$ eV has been

taken in the calculation to be consistent with the results obtained by the *ab initio* calculations [17, 18, 29].

Discussion.— There are several experimental evidences that may support the idea that the intralayer ferromagnetic order becomes much smaller and more localized in real materials. The diminishment of the intralayer ferromagnetic order has been justified in recent experiments as the Mn atomic magnetic moment is about $1.14 \mu_B$ in MnBi_2Te_4 thin films [19] and around $3.8 \mu_B$ in bulk MnBi_2Te_4 [23], which is much smaller than the theoretically expected values of $4.6 \mu_B$ [16, 29] or $5 \mu_B$ [18, 19]. Moreover, the resonance photoemission spectroscopy measurements have revealed that the density of Mn 3d states is negligible in the energy range within 0.6 eV below the Fermi energy [21, 22], which is similar to that in Mn-doped Sb_2Te_3 [48]. This implies a local nature of the Mn 3d states in MnBi_2Te_4 [21, 22].

This work was supported by the National Natural Science Foundation of China (Grant No. 11534001, No. 11974249, and No. 11925402), the Strategic Priority Research Program of Chinese Academy of Sciences (Grant No. XDB28000000), Guangdong province (Grant No. 2016ZT06D348, and No. 2020KCXTD001), the National Key R & D Program (Grant No. 2016YFA0301700), the Natural Science Foundation of Shanghai (Grant No. 19ZR1437300), Shenzhen High-level Special Fund (Grant No. G02206304, and No. G02206404), and the Science, Technology and Innovation Commission of Shenzhen Municipality (No. ZDSYS20170303165926217, No. JCYJ20170412152620376, and No. KYTDPT20181011104202253). The numerical calculations were supported by Center for Computational Science and Engineering of Southern University of Science and Technology.

Y. Kozuka, K. S. Takahashi, M. Kawasaki, and Y. Tokura, “Magnetic modulation doping in topological insulators toward higher-temperature quantum anomalous Hall effect”, *Appl. Phys. Lett.* **107**, 182401 (2015).

- [9] Y. Tokura, K. Yasuda, and A. Tsukazaki, “Magnetic topological insulators”, *Nat. Rev. Phys.* **1**, 126 (2019).
- [10] M. M. Otkrov, T. V. Menshchikova, I. P. Rusinov, M. G. Vergniory, V. M. Kuznetsov, and E. V. Chulkov, “Magnetic extension as an efficient method for realizing the quantum anomalous Hall state in topological insulators”, *JETP Lett.* **105**, 297 (2017).
- [11] M. M. Otkrov, T. V. Menshchikova, M. G. Vergniory, I. P. Rusinov, A. Y. Vyazovskaya, Y. M. Koroteev, G. Bihlmayer, A. Ernst, P. M. Echenique, A. Arnau, *et al.*, “Highly-ordered wide bandgap materials for quantized anomalous Hall and magnetoelectric effects”, *2D Mater.* **4**, 025082 (2017).
- [12] R. S. K. Mong, A. M. Essin, and J. E. Moore, “Antiferromagnetic topological insulators”, *Phys. Rev. B* **81**, 245209 (2010).
- [13] S. Chowdhury, K. F. Garrity, and F. Tavazza, “Prediction of Weyl semimetal and antiferromagnetic topological insulator phases in Bi_2MnSe_4 ”, *npj Comput. Mater.* **5**, 33 (2019).
- [14] R. S. Mong and J. E. Moore, “Magnetic and topological order united in a crystal”, *Nature (London)* **576**, 390 (2019).
- [15] E. D. L. Rienks, S. Wimmer, J. Sánchez-Barriga, O. Caha, P. S. Mandal, J. Ruzicka, A. Ney, H. Steiner, V. V. Volobuev, H. Groiss, *et al.*, “Large magnetic gap at the dirac point in $\text{Bi}_2\text{Te}_3/\text{MnBi}_2\text{Te}_4$ heterostructures”, *Nature (London)* **576**, 423 (2019).
- [16] M. M. Otkrov, I. I. Klimovskikh, H. Bentmann, D. Estyulin, A. Zeugner, Z. S. Aliev, S. Gaß, A. U. B. Wolter, A. V. Koroleva, A. M. Shikin, *et al.*, “Prediction and observation of an antiferromagnetic topological insulator”, *Nature (London)* **576**, 416 (2019).
- [17] D. Zhang, M. Shi, T. Zhu, D. Xing, H. Zhang, and J. Wang, “Topological axion states in the magnetic insulator MnBi_2Te_4 with the quantized magnetoelectric effect”, *Phys. Rev. Lett.* **122**, 206401 (2019).
- [18] J. Li, Y. Li, S. Du, Z. Wang, B.-L. Gu, S.-C. Zhang, K. He, W. Duan, and Y. Xu, “Intrinsic magnetic topological insulators in van der Waals layered MnBi_2Te_4 -family materials”, *Sci. Adv.* **5**, eaaw5685 (2019).
- [19] Y. Gong, J. Guo, J. Li, K. Zhu, M. Liao, X. Liu, Q. Zhang, L. Gu, L. Tang, X. Feng, *et al.*, “Experimental realization of an intrinsic magnetic topological insulator”, *Chin. Phys. Lett.* **36**, 076801 (2019).
- [20] B. Chen, F. Fei, D. Zhang, B. Zhang, W. Liu, S. Zhang, P. Wang, B. Wei, Y. Zhang, Z. Zuo, *et al.*, “Intrinsic magnetic topological insulator phases in the Sb doped MnBi_2Te_4 bulks and thin flakes”, *Nat. Commun.* **10**, 4469 (2019).
- [21] R. C. Vidal, H. Bentmann, T. R. F. Peixoto, A. Zeugner, S. Moser, C.-H. Min, S. Schatz, K. Kibler, M. Ünzelmann, C. I. Fornari, *et al.*, “Surface states and Rashba-type spin polarization in antiferromagnetic $\text{MnBi}_2\text{Te}_4(0001)$ ”, *Phys. Rev. B* **100**, 121104(R) (2019).
- [22] H. Li, S.-Y. Gao, S.-F. Duan, Y.-F. Xu, K.-J. Zhu, S.-J. Tian, J.-C. Gao, W.-H. Fan, Z.-C. Rao, J.-R. Huang, *et al.*, “Dirac surface states in intrinsic magnetic topological insulators EuSn_2As_2 and $\text{MnBi}_{2n}\text{Te}_{3n+1}$ ”, *Phys. Rev. X* **9**, 041039 (2019).

* Corresponding author: luhz@sustech.edu.cn

- [1] J. E. Moore, “The birth of topological insulators”, *Nature (London)* **464**, 194 (2010).
- [2] M. Z. Hasan and C. L. Kane, “Colloquium: Topological insulators”, *Rev. Mod. Phys.* **82**, 3045 (2010).
- [3] X.-L. Qi and S.-C. Zhang, “Topological insulators and superconductors”, *Rev. Mod. Phys.* **83**, 1057 (2011).
- [4] S.-Q. Shen, *Topological Insulators* (Springer-Verlag, Berlin, 2012).
- [5] C.-X. Liu, X.-L. Qi, X. Dai, Z. Fang, and S.-C. Zhang, “Quantum anomalous Hall effect in $\text{Hg}_{1-y}\text{Mn}_y\text{Te}$ quantum wells”, *Phys. Rev. Lett.* **101**, 146802 (2008).
- [6] R. Yu, W. Zhang, H.-J. Zhang, S.-C. Zhang, X. Dai, and Z. Fang, “Quantized anomalous Hall effect in magnetic topological insulators”, *Science* **329**, 61 (2010).
- [7] C.-Z. Chang, J. Zhang, X. Feng, J. Shen, Z. Zhang, M. Guo, K. Li, Y. Ou, P. Wei, L.-L. Wang, *et al.*, “Experimental observation of the quantum anomalous Hall effect in a magnetic topological insulator”, *Science* **340**, 167 (2013).
- [8] M. Mogi, R. Yoshimi, A. Tsukazaki, K. Yasuda,

- [23] Y.-J. Hao, P. Liu, Y. Feng, X.-M. Ma, E. F. Schwier, M. Arita, S. Kumar, C. Hu, R. Lu, M. Zeng, *et al.*, “Gapless surface Dirac cone in antiferromagnetic topological insulator MnBi₂Te₄”, *Phys. Rev. X* **9**, 041038 (2019).
- [24] Y. J. Chen, L. X. Xu, J. H. Li, Y. W. Li, H. Y. Wang, C. F. Zhang, H. Li, Y. Wu, A. J. Liang, C. Chen, *et al.*, “Topological electronic structure and its temperature evolution in antiferromagnetic topological insulator MnBi₂Te₄”, *Phys. Rev. X* **9**, 041040 (2019).
- [25] P. Swatek, Y. Wu, L.-L. Wang, K. Lee, B. Schrunk, J. Yan, and A. Kaminski, “Gapless Dirac surface states in the antiferromagnetic topological insulator MnBi₂Te₄”, *Phys. Rev. B* **101**, 161109(R) (2020).
- [26] Y. Deng, Y. Yu, M. Z. Shi, Z. Guo, Z. Xu, J. Wang, X. H. Chen, and Y. Zhang, “Quantum anomalous Hall effect in intrinsic magnetic topological insulator MnBi₂Te₄”, *Science* **367**, 895 (2020).
- [27] C. Liu, Y. Wang, H. Li, Y. Wu, Y. Li, J. Li, K. He, Y. Xu, J. Zhang, and Y. Wang, “Robust axion insulator and Chern insulator phases in a two-dimensional antiferromagnetic topological insulator”, *Nat. Mater.* **19**, 522 (2020).
- [28] J. Ge, Y. Liu, J. Li, H. Li, T. Luo, Y. Wu, Y. Xu, and J. Wang, “High-Chern-number and high-temperature quantum Hall effect without Landau levels”, *Nat. Sci. Rev.* **7**, 1280 (2020).
- [29] M. M. Otkov, I. P. Rusinov, M. Blanco-Rey, M. Hoffmann, A. Y. Vyazovskaya, S. V. Eremeev, A. Ernst, P. M. Echenique, A. Arnau, and E. V. Chulkov, “Unique thickness-dependent properties of the van der Waals interlayer antiferromagnet MnBi₂Te₄ films”, *Phys. Rev. Lett.* **122**, 107202 (2019).
- [30] J. Li, C. Wang, Z. Zhang, B.-L. Gu, W. Duan, and Y. Xu, “Magnetically controllable topological quantum phase transitions in the antiferromagnetic topological insulator MnBi₂Te₄”, *Phys. Rev. B* **100**, 121103(R) (2019).
- [31] J. Wu, F. Liu, M. Sasase, K. Ienaga, Y. Obata, R. Yukawa, K. Horiba, H. Kumigashira, S. Okuma, T. Inoshita, *et al.*, “Natural van der Waals heterostructural single crystals with both magnetic and topological properties”, *Sci. Adv.* **5**, eaax9989 (2019).
- [32] A. Zeugner, F. Nietschke, A. U. B. Wolter, S. Gaß, R. C. Vidal, T. R. F. Peixoto, D. Pohl, C. Damm, A. Lubk, R. Henrich, *et al.*, “Chemical aspects of the candidate antiferromagnetic topological insulator MnBi₂Te₄”, *Chem. Mater.* **31**, 2795 (2019).
- [33] S. H. Lee, Y. Zhu, Y. Wang, L. Miao, T. Pillsbury, H. Yi, S. Kempinger, J. Hu, C. A. Heikes, P. Quarterman, *et al.*, “Spin scattering and noncollinear spin structure-induced intrinsic anomalous hall effect in antiferromagnetic topological insulator MnBi₂Te₄”, *Phys. Rev. Research* **1**, 012011(R) (2019).
- [34] A. M. Shikin, D. A. Estyunin, I. I. Klimovskikh, S. O. Fil'nov, E. F. Schwier, S. Kumar, K. Miyamoto, T. Okuda, A. Kimura, K. Kuroda, *et al.*, “Nature of the Dirac gap modulation and surface magnetic interaction in axion antiferromagnetic topological insulator MnBi₂Te₄”, *Sci. Rep.* **10**, 13226 (2020).
- [35] V. N. Men'shov, V. V. Tugushev, and E. V. Chulkov, “Quantum anomalous Hall effect in magnetically modulated topological insulator/normal insulator heterostructures”, *JETP Lett.* **104**, 453 (2016).
- [36] H. Z. Lu, W. Y. Shan, W. Yao, Q. Niu, and S. Q. Shen, “Massive Dirac fermions and spin physics in an ultrathin film of topological insulator”, *Phys. Rev. B* **81**, 115407 (2010).
- [37] W.-Y. Shan, H.-Z. Lu, and S.-Q. Shen, “Effective continuous model for surface states and thin films of three-dimensional topological insulators”, *New J. Phys.* **12**, 043048 (2010).
- [38] Y. Zhang, K. He, C.-Z. Chang, C.-L. Song, L.-L. Wang, X. Chen, J.-F. Jia, Z. Fang, X. Dai, W.-Y. Shan, *et al.*, “Crossover of the three-dimensional topological insulator Bi₂Se₃ to the two-dimensional limit”, *Nat. Phys.* **6**, 584 (2010).
- [39] C. M. Wang, H.-P. Sun, H.-Z. Lu, and X. C. Xie, “3D quantum Hall effect of Fermi arcs in topological semimetals”, *Phys. Rev. Lett.* **119**, 136806 (2017).
- [40] C. Zhang, Y. Zhang, X. Yuan, S. Lu, J. Zhang, A. Narayan, Y. Liu, H. Zhang, Z. Ni, R. Liu, *et al.*, “Quantum Hall effect based on Weyl orbit in Cd₃As₂”, *Nature (London)* **565**, 331 (2019).
- [41] P. Villars and K. Cenzual, “Bi₂MnTe₄ (MnBi₂Te₄) crystal structure: Datasheet from PAULING FILE Multinarines Edition – 2012”, *Springer Materials*.
- [42] J.-Q. Yan, Q. Zhang, T. Heitmann, Z. Huang, K. Y. Chen, J.-G. Cheng, W. Wu, D. Vaknin, B. C. Sales, and R. J. McQueeney, “Crystal growth and magnetic structure of MnBi₂Te₄”, *Phys. Rev. Materials* **3**, 064202 (2019).
- [43] See Supplemental Material at <http://link.aps.org/supplemental/10.1103/PhysRevB.102.241406> for the detailed calculations.
- [44] S. V. Eremeev, M. G. Vergniory, T. V. Menshchikova, A. A. Shaposhnikov, and E. V. Chulkov, “The effect of van der Waal's gap expansions on the surface electronic structure of layered topological insulators”, *New J. Phys.* **14**, 113030 (2012).
- [45] Y. Yuan, X. Wang, H. Li, J. Li, Y. Ji, Z. Hao, Y. Wu, K. He, Y. Wang, Y. Xu, *et al.*, “Electronic states and magnetic response of MnBi₂Te₄ by scanning tunneling microscopy and spectroscopy”, *Nano Lett.* **20**, 3271 (2020).
- [46] Z. Liang, A. Luo, M. Shi, Q. Zhang, S. Nie, J. J. Ying, J.-F. He, T. Wu, Z. Wang, G. Xu, *et al.*, “Mapping Dirac fermions in the intrinsic antiferromagnetic topological insulators (MnBi₂Te₄)(Bi₂Te₃)_n (n = 0, 1)”, *Phys. Rev. B* **102**, 161115(R) (2020).
- [47] W. Zhang, R. Yu, H.-J. Zhang, X. Dai, and Z. Fang, “First-principles studies of the three-dimensional strong topological insulators Bi₂Te₃, Bi₂Se₃ and Sb₂Te₃”, *New J. Phys.* **12**, 065013 (2010).
- [48] M. F. Islam, C. M. Canali, A. Pertsova, A. Balatsky, S. K. Mahatha, C. Carbone, A. Barla, K. A. Kokh, O. E. Tereshchenko, E. Jiménez, *et al.*, “Systematics of electronic and magnetic properties in the transition metal doped Sb₂Te₃ quantum anomalous Hall platform”, *Phys. Rev. B* **97**, 155429 (2018).